

Detail-preserving Mesh Unfolding for Non-rigid Shape Retrieval

YUSUF SAHILLIOĞLU

Computer Engineering Department, Middle East Technical University, Turkey

and

LADISLAV KAVAN

School of Computing, University of Utah, USA

We present a shape deformation algorithm that unfolds any given 3D shape into a canonical pose that is invariant to non-rigid transformations. Unlike classical approaches, such as least-squares multidimensional scaling, we preserve the geometric details of the input shape in the resulting shape, which in turn leads to a content-based non-rigid shape retrieval application with higher accuracy. Our optimization framework, fed with a triangular or a tetrahedral mesh in 3D, tries to move each vertex as far away from each other as possible subject to finite element regularization constraints. Intuitively this effort minimizes the bending over the shape while preserving the details. Avoiding geodesic distances in our computation renders the method robust to topological noise. Compared to state-of-the-art approaches, our method is simpler to implement, faster, more accurate in shape retrieval, and less sensitive to topological errors.

Categories and Subject Descriptors: I.3.5 [Computer Graphics]: Computational Geometry and Object Modeling—*Curve, surface, solid, and object representations*

General Terms: Shape Representation, Shape Retrieval

Additional Key Words and Phrases: Canonical pose, detail preservation, non-rigid shape retrieval

1. INTRODUCTION

3D shapes are the building blocks of many computer graphics and vision applications ranging from interpolation [Freifeld and Black 2012] to deformation [Nealen et al. 2006]. Consequently it is important to find the best representation of these shapes tailored to the specific application in mind. In this paper, we will introduce a new canonical representation that is shown to be more advantageous for the shape retrieval application.

Thanks to the increasing sizes and numbers of 3D model repositories, the task of fast and robust retrieval of shapes never loses

attention [Li et al. 2014]. Our new canonical shape representation facilitates a scalable search algorithm that is shown to be effective on 3D shape databases of articulated, or equivalently non-rigid, objects. Existing approaches essentially address this problem by performing 3D non-rigid shape comparisons using i) descriptors, ii) global intrinsic properties, or iii) canonical forms, where the last option is the most promising one as the canonical form can easily be integrated into a simpler and well-studied rigid shape retrieval process. Despite this advantage, there has been few canonical forms proposed in the literature. Moreover, all but the most recent one [Lian et al. 2013] are based on embedding procedures that introduce serious distortions (Fig. 1). The feature-preserving canonical form of [Lian et al. 2013] has obtained significantly better retrieval accuracy than the state-of-the-art canonical methods. This is due to the fact that semantically similar objects with varying geometric details could not be well distinguished by a canonical pose that distorts details. Our algorithm, compared to this closest work [Lian et al. 2013], is simpler to implement, faster, more accurate in shape retrieval, and less sensitive to topological noise. In addition to this main contribution, our canonical pose simplifies texture mapping and allows geodesic distance approximation by revealing the extrinsic properties of the shapes.

In order to compute the detail-preserving canonical pose from a given arbitrary pose, we formulate an optimization problem whose solution separates each mesh vertex as far as possible while preserving the geometric details of the original shape such as the bumps and cavities on the surface. Hence we promote a pose with minimum bending and maximum geometric detail.

The source code and the executables for the method that we present in this paper are publicly available at <http://www.ceng.metu.edu.tr/~ys/pubs>.

2. RELATED WORK

Shape retrieval is an important problem coming in various scenarios based on the query paradigms as well as the supported deformations between the query and the database models [Tangelder and Veltkamp 2008]. The former includes query-by-keyword, query-by-sketch, query-by-example, or a combined usage, whereas the latter determines the similarity measure to be considered while matching the query with the database models; popular ones being rigid matching and non-rigid matching. We address 3D shape retrieval with non-rigid matching and query-by-example setting, meaning that an example shape in arbitrary pose will be non-rigidly matched to the database models with the hope of returning the semantically similar objects to the user.

Shape representation issue is closely related to the shape retrieval problem. One may represent the exemplar query shape and the database shapes with global descriptors to convert the problem into a lower-dimensional and hence simpler descriptor matching problem. The popular descriptors that are invariant to rigid trans-

Authors' addresses: Yusuf Sahillioğlu, (Current address) CENG METU, Universiteler Mah. Dumlupınar Blv. No:1, Ankara, Turkey.

Permission to make digital or hard copies of part or all of this work for personal or classroom use is granted without fee provided that copies are not made or distributed for profit or commercial advantage and that copies show this notice on the first page or initial screen of a display along with the full citation. Copyrights for components of this work owned by others than ACM must be honored. Abstracting with credit is permitted. To copy otherwise, to republish, to post on servers, to redistribute to lists, or to use any component of this work in other works requires prior specific permission and/or a fee. Permissions may be requested from Publications Dept., ACM, Inc., 2 Penn Plaza, Suite 701, New York, NY 10121-0701 USA, fax +1 (212) 869-0481, or permissions@acm.org.

© YYYY ACM 0730-0301/YYYY/16-ARTXXX \$10.00

DOI 10.1145/XXXXXXXX.YYYYYYY

<http://doi.acm.org/10.1145/XXXXXXXX.YYYYYYY>

formations, i.e., translations and rotations, for rigid shape retrieval are spin images [Johnson and Hebert 1999; Assfalg et al. 2007], wavelets [Paquet et al. 2000], statistical moments [Zhang and Chen 2001; Novotni and Klein 2003], shape contexts [Belongie et al. 2002], shape distributions [Osada et al. 2002], spherical harmonics [Funkhouser et al. 2003; Kazhdan et al. 2003], and lightfield descriptor [Chen et al. 2003]. Note that, [Funkhouser et al. 2003] and [Chen et al. 2003] allow sketch queries as part of their example-based retrieval engines for rigid shapes. Alternatively rigid shape retrieval problem may be solved by efficiently registering the query to each database models in the low-dimensional space of rigid transformations [Besl and Mckay 1992]. The initial guess for [Besl and Mckay 1992] can always be improved by the fast PCA-based alignment [Kazhdan 2007]. A simple correspondence based on the closest points of the registered pair would then yield a cost descriptor that is useful for retrieval purposes.

For the non-rigid shape retrieval, which is more generic than the rigid counterpart, the existing methods are based on i) articulation-invariant descriptors, ii) global intrinsic properties, or iii) articulation-invariant postures, a.k.a. the canonical poses. The descriptors here are invariant to non-rigid transformations, i.e., rigid transformations plus bending. Laplace-Beltrami differential operator is used extensively in the formulation of these descriptors [Reuter et al. 2006; Sun et al. 2009; Zaharescu et al. 2009; Bronstein and Kokkinos 2010; Raviv et al. 2010; Bronstein et al. 2011]. A global intrinsic property for all non-rigid shapes is the geodesic distance, which is consequently a good clue for non-rigid matching. Many algorithms exploit the preservation of geodesic distances under non-rigid transformations in order to utilize descriptors [Mahmoudi and Sapiro 2009] or graphs [Hilaga et al. 2001; Barra and Biasotti 2013] for non-rigid shape retrieval. Another important usage of the geodesic distances is the creation of canonical poses that are invariant to non-rigid transformations. In the canonical pose, the Euclidean distance between any two surface points approximates the geodesic distance between the corresponding vertices in the original pose. This idea is realized with the classical multidimensional scaling (MDS) method [Gower 1966; Jain and Zhang 2007] where the leading eigenvectors of the geodesic affinity matrix define the canonical pose. A similar pose is achieved with the least-squares MDS where a similar objective function is minimized [Elad and Kimmel 2003; Au et al. 2010]. Both of these MDS procedures require dense geodesic distance computations [Crane et al. 2013] which render them inappropriate for high-resolution meshes. [de Silva and Tenenbaum 2002; Panozzo et al. 2013] address this issue by finding geodesics only for the few landmark points and interpolating the result for the remaining data points. Another problem with the geodesic-based MDS methods is their vulnerability to the topological noise as a small modification on shape connectivity may change geodesics, i.e., the shortest paths, drastically. To remedy this problem [Rustamov 2007] proposes a canonical pose based on Laplace-Beltrami eigenfunctions, whose sign and order switch issue, however, poses another problem. [Lipman and Funkhouser 2009] also avoids the use of geodesic distances by conformally mapping shapes with sphere topology into the extended complex plane via Möbius embedding. All these canonical poses exhibit significant distortions as it is impossible to satisfy all pairwise distances simultaneously in the restricted flat Euclidean space [Bronstein et al. 2008]. In order to eliminate the distortion, [Bronstein et al. 2006] proposes to embed one of the shapes to be matched into the surface of the other via the generalized MDS, which requires minimization of a non-convex stress function. Due to the heavy computational complexity involved, generalized MDS is presented as a solution for the shape correspondence problem that deals with

only two shapes, rather than the problem of shape retrieval from large databases. Given plenty of execution time, generalized MDS, as well as the other non-rigid shape correspondence algorithms [Jain and Zhang 2006; Ovsjanikov et al. 2010; Sahillioğlu and Yemez 2012; 2013], may be utilized to address the retrieval problem as the correspondence cost defines a plausible similarity measure.

Among the three types of non-rigid shape retrieval methods discussed above, namely i) descriptor-based, ii) intrinsic-based, and iii) canonical, the last one is generally promoted as the most promising approach because by definition all shapes of the same class converges to the same canonical pose up to rigid transformations. This makes all the simpler and well-acknowledged rigid retrieval techniques available for the non-rigid retrieval problem, which is a big win. It is then natural to seek for improvements on the detail-oblivious canonical representation as objects of the same class with varying geometric details could not be distinguished sufficiently in the original setting. The first work addressing this issue to some extent is [Lian et al. 2013], which deforms near-rigid mesh segments towards the corresponding components on the distorted least-squares MDS canonical pose. Although details are preserved to some extent, segmentation errors on the surface cause problems on the output shape (Fig. 12). Besides the computational cost is too expensive for real search engines and the method is sensitive to topological errors. Their resulting detail-preserving canonical pose, on the other hand, performs much better than the detail-oblivious canonical poses for non-rigid shape retrieval purposes, as expected. We are inspired by this improvement and introduce our detail-preserving 3D canonical posing algorithm which produces a smoother and more accurate unfolding in a smaller amount of time than that of [Lian et al. 2013], hence improving their good retrieval performance even further. We also note that we avoid geodesic distances in our computations for a scalable method that is also robust to topological noises. Thanks to the simple closed form of our deformation model, our algorithm is not only efficient but also easy to implement. We finally note that in a concurrent work [Sahillioğlu 2015] obtains a detail-preserving canonical form by treating the vertices of the Landmark MDS embedding [de Silva and Tenenbaum 2002] as handles to deform the original shape. However, their work employs the problematic geodesic distances and a simpler yet faster deformation regularization energy. Instead, we do not use geodesics and achieve regularization with a more sophisticated scheme based on springs and the finite element method, which in turn achieves more accurate results in terms of element inversions and retrieval performance.

Our method is based on shape deformation, which allows us to explicitly control the geometric details of the shapes, a property that is lacking in all the embedding-based canonical pose creation methods. There are different deformation energies that guide shape deformation by measuring the difference between the current deformed configuration and the initial fixed rest-pose [Nealen et al. 2006; Botsch and Sorkine 2008]. The most basic one is the Dirichlet energy [Bonet and Wood 1997] that penalizes rotations and consequently allows only small deviations from the initial pose. Green's strain energy [Bonet and Wood 1997] allows not only the proper rotations but also the improper ones, i.e., reflections, which in turn enables a better separation from the initial pose while permitting undesired element inversions. This problem is handled in the state-of-the-art deformation energies that facilitate large deformations with no or very few inverted elements [Irving et al. 2004; Muller et al. 2005; Sorkine and Alexa 2007; Liu et al. 2008; Chao et al. 2010; Stomakhin et al. 2012].

Deformation energies become more interesting when they are coupled with positioning and regularization constraints. In interactive shape deformation, for instance, user specifies the position of the manipulation handles as the positioning constraints that work against the deformation energy [Sorkine et al. 2004]. Regularization constraints, on the other hand, try to keep the mesh in good shape during the whole deformation process. They essentially help the deformation energy term by additional soft or hard specifications on some regional properties such as angle, area, and volume [Muller et al. 2004; Irving et al. 2007; Adams et al. 2008; Schuller et al. 2013]. We adapt the composite element approach of [Irving et al. 2007] which enforces constant volume in one-ring of each vertex.

Finally, we mention the special poses in the literature that are used for tasks other than shape retrieval. A commonality of all these poses is that the geometric details are preserved. [Mitra et al. 2007], for instance, strives to bring a given arbitrary pose into a special pose, which is in their case the symmetrized pose that enhances Euclidean symmetries present in the input. They find the symmetrizing transformation based on a set of corresponding symmetric point pairs computed by a curvature-based search algorithm. [Twigg and Kačić-Alesić 2011] approximately compensates the mesh sagging effect under gravity by estimating rest-length parameters of a spring-mass system. Inverse design methods in [Skouras et al. 2012; Chen et al. 2014] aim to compute a rest-shape for 3D printing, which can deform into the desired target shape under specified forces when fabricated. Based on the concepts of electrostatics, [Wang et al. 2013] achieves spherical surface parameterization for shapes with arbitrary topology.

3. ALGORITHM

In this section we describe our shape deformation algorithm for canonical pose optimization. Deformation is defined as a change in the shape or pose of an object due to applied forces. In other words, deformation is a mapping from \mathbb{R}^m to \mathbb{R}^m , where we consider $m = 3$ in this work.

The input to our system is an elastic 2D triangular surface embedded in \mathbb{R}^3 . For more realistic results, we consider volumetric elasticity, which requires tetrahedralizing the entire volume of the input surface [Jacobson et al. 2013]. After this preprocessing, we denote with $V = \{1, 2, \dots, n\}$ and $E = \{1, 2, \dots, e\}$ the set of vertex and edge indices, respectively. The position of vertex i of our tetrahedral mesh M is given by \mathbf{v}_i .

Our task is to bring M into its canonical pose, which can be realized by minimizing the bending on it while conserving the shape details. The problem can then be formulated as a search over all possible vertex locations so as to minimize a convenient energy functional $E(\mathbf{v})$:

$$\mathbf{v}^* = \arg \min_{\mathbf{v}} E(\mathbf{v}). \quad (1)$$

The search space is reduced by exploiting the fact that the optimal locations \mathbf{v}^* for a bending-free pose move every vertex as far away from each other as possible while keeping M in good shape with full original details. This is equivalent to detail-preserving unfolding of the input mesh. In the following we derive our $E(\mathbf{v})$ that addresses this requirement.

3.1 Canonical Pose Optimization Energy

We start with the simplest energy function:

$$E(\mathbf{v}) = \sum_{i < j} (\|\mathbf{v}_i - \mathbf{v}_j\| - g(i, j))^2, \quad (2)$$

where $g(\cdot, \cdot)$ is the geodesic distance between two vertices on a given surface. This is a mass-spring system, arguably the simplest deformation model consisting of point masses connected together by massless springs. Spring forces are governed by Hooke's law. See [Nealen et al. 2006] for a more detailed discussion. Our mass-spring system in Eq. 2 consists of V as masses and the so-called geodesic springs that run between all pairs of vertices $\{(i, j) | i < j\} \in V$. Minimization of this energy makes the lengths of the geodesic springs close to the corresponding pairwise geodesic distances, which effectively separates any given point by the amount of the geodesic distance in between. This is indeed a well-known Euclidean embedding method, Multidimensional Scaling (MDS), that comes in least-squares form [Elad and Kimmel 2003]. The primary purpose of the MDS methods is to represent the pairwise (dis)similarity data, e.g., geodesic distances, as Euclidean distances in a low-dimensional space in order to make it accessible to visual inspection and further exploration. Since MDS methods do not utilize any information other than the pairwise data, they are very likely to lose the geometric details of the input in the resulting embedding, as exemplified in Fig. 1 (see also Figures 7-9 and 12 for outputs of different types of MDS method).

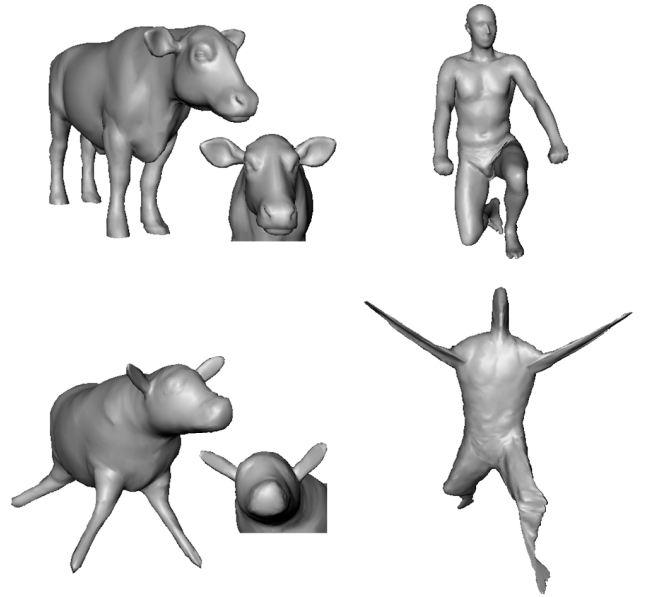


Fig. 1. Original shapes (top row) unfolded by minimization of Eq. 2, or equivalently, by the least-squares MDS method [Elad and Kimmel 2003] (bottom row). Note the loss of details.

In order to alleviate the detail-preservation problem of Eq. 2, we add new springs to our existing mass-spring system:

$$E(\mathbf{v}) = \frac{1}{2} \sum_{(i, j) \in \mathcal{G} \cup \mathcal{E}} k_{ij} (\|\mathbf{v}_i - \mathbf{v}_j\| - r_{ij})^2, \quad (3)$$

where the spring set is the union of the geodesic springs \mathcal{G} (between all pairs of vertices $\{(i, j) | i < j\} \in V$) and the so-called edge springs \mathcal{E} (between connected pairs of vertices $(i, j) \in E$), and k_{ij} is the spring stiffness. The rest length r_{ij} takes the value of geodesic distance (for geodesic springs) or original edge length (for edge springs).

The problem with Eq. 3 is its dependence on the original geodesic distances and the pure spring-based approach to capture volumetric elasticity (see Fig. 2-b). Geodesic distances require significant time and storage complexity for high-resolution meshes. More importantly, since we expect some stretching in the unfolded pose that we aim for, original geodesic distances should alter in an unpredictable manner. Therefore, we remove geodesic distances entirely from our system and employ a charge-based method (Eq. 4). With springs, on the other hand, it is very difficult to control the compressibility of a tetrahedron, and also impossible to detect inversions. Setting stiffness parameters for non-uniformly tessellated meshes is yet another issue. Therefore, we add the support for the finite element method, representing a principled approach to address these problems (Eqs. 5 and 6).

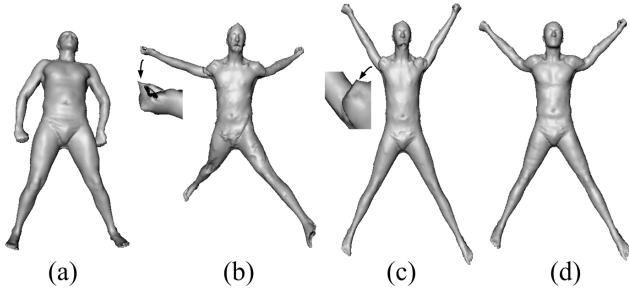


Fig. 2. Original mesh (a) and its canonical pose due to Eq. 3 (b), Eq. 4 (c), and Eq. 4 with constraints (d). Inverted or highly-distorted parts are zoomed in.

Our proposed energy function for the canonical pose computation is as follows:

$$E(\mathbf{v}) = \frac{1}{2} \left(\sum_{(i,j) \in \mathcal{C}} -k_{ij} \|\mathbf{v}_i - \mathbf{v}_j\|^2 + \alpha \sum_{(i,j) \in \mathcal{E}} k_{ij} (\|\mathbf{v}_i - \mathbf{v}_j\| - r_{ij})^2 \right), \quad (4)$$

where \mathcal{C} denotes the charge springs (between all pairs of vertices $\{(i,j) | i < j\} \in V$), \mathcal{E} is the set of edge springs as before, k_{ij} is the spring stiffness, and α is a tuning parameter controlling the effect of the edge springs. Spring stiffness value k_{ij} is always 1 in this paper. We control the regularization effect with α parameter, and elaborate on the choice of α in Sec. 4.2.2. The rest length r_{ij} is the original edge length for edge springs, and equal to 0 for charge springs. The charge springs essentially maximize the distance between vertex pairs by minimizing the negative distance between them. The name charge comes from the fact that identically charged particles repulse each other in electric fields, just like our vertices V repulsing each other. To summarize, edge springs help detail-preservation whereas charge springs are responsible for the unfolding operation. The main reason of the success of the proposed energy function (Eq. 4) over the original one (Eq. 2) is the elimination of unpredictable geodesic distances in the unfolded pose. Another advantage is time and storage efficiency as well as topological noise robustness (Fig. 13) obtained by ruling out geodesic computations. We visualize the charge and edge springs on a didactic example in Fig. 3. See also Fig. 2-c and Fig. 6-right to see an input pose and the resulting canonical pose based on these springs.

Although our final energy in Eq. 4 is free of geodesic distances and hence the associated problems, it still involves regularization problems due to springs as shown in Fig. 2-c (see also Fig. 6-right). We address this issue by minimizing Eq. 4 subject to finite element

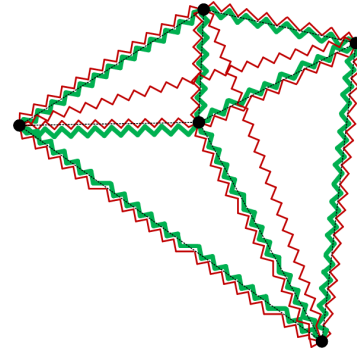


Fig. 3. A 2D mesh with 5 vertices and 8 edges has $\binom{5}{2} = 10$ charge springs (red) and 8 edge springs (bold green). Edge springs are generally stiffer to better control the repulsing effect of the charge springs, e.g., edge springs prevent the vertical charge spring (the longest one) from separating the top and the bottom vertices by infinite distance.

constraints. The first set of constraints is responsible for preserving local volume around each vertex:

$$c_i(\mathbf{v}) : \sum_{t \in \eta(i)} \text{vol}(t) = l_i \quad \forall i \in V, \quad (5)$$

where $\eta(i)$ are the tetrahedra indices in the one-ring neighborhood of vertex i , function $\text{vol}(t)$ measures the volume of t , and l_i is the initial local volume around i in the original pose. Note that this is the one-ring composite element constraint in [Irving et al. 2007], which avoids locking, i.e., the inability of a given overconstrained finite element space to approximate solutions. The second set of constraints are inequalities to prevent inversions:

$$c_t(\mathbf{v}) : \text{vol}(t) > \epsilon \quad \forall t \in T, \quad (6)$$

where T is the set all tetrahedra indices and ϵ is a small constant for numerical inaccuracies, being one-hundredth of the minimum volume of all the original tetrahedra. These two sets of constraints along with the edge springs achieve a nice regularization effect, which we visualize in Fig. 2-d (see also Fig. 6-middle). Note that, edge springs are still a fundamental part of our formulation as they prevent constraints from being satisfied with arbitrary edge lengths. In addition to or in place of Eqs. 5 and 6, we have also tried another constraint candidate, which preserves the local edge length summation around each vertex, i.e., sum of lengths of the edges incident to a vertex is preserved, and yet not observed any improvement. For an efficient solution of our nonlinear constrained optimization problem, we have employed the interior-point method implemented in a state-of-the-art KNITRO solver [Byrd et al. 2006]. Specifically, we solve the following constrained optimization problem:

$$\begin{aligned} & \underset{\mathbf{v}}{\text{minimize}} && E(\mathbf{v}) \\ & \text{subject to} && c_i(\mathbf{v}), \forall i \in V \quad \text{and} \quad c_t(\mathbf{v}), \forall t \in T. \end{aligned}$$

4. EXPERIMENTAL RESULTS

4.1 Datasets

We demonstrate the potential of our detail-preserving mesh unfolding algorithm in a content-based non-rigid shape retrieval application. To this end, we use Watertight [Giorgi et al. 2007], McGill [Siddiqi et al. 2008], and SCAPE [Angelov et al. 2005] datasets,

union of which forms a large database of 507 models with articulating parts. We query this database using random individual models selected from the database itself. The part that we have used from the Watertight benchmark consists of glasses, ant, chair, octopus, table, fish, rope, armadillo, and fourleg classes of cardinality 20 each. The remaining 11 classes have been omitted due to uninteresting type and/or pose of their constituent elements. We have used all the 256 articulated models in the McGill database consisting of various classes ranging from humans to spiders. SCAPE dataset, on the other hand, is a reconstructed sequence of a human actor in 71 different fixed-connectivity poses. Models in both datasets are non-uniformly sampled. We have also used the hand model from [Panozzo et al. 2013] to compare with their embedding result. As a side application, we also demonstrate our geodesic distance approximation capability on the SCAPE and Watertight models.

4.2 Evaluation Criteria

We evaluate the quality of our resulting canonical poses visually (Figures 4-8) and quantitatively, namely in terms of the amount of stretching (Table I-first row), geodesic distance approximation accuracy (Fig. 9, Table I-second row), and non-rigid retrieval performance (Figures 10-11, Tables II-IV). We also compare our canonical poses and their retrieval performance with the state-of-the-art approaches in Sec. 4.2.3.

4.2.1 Visual Evaluation. In Figures 4-5, we see the detail-preserving unfolding of example models from various Watertight classes, whereas in Fig. 6 we show the benefit of our local volume preservation and inversion prevention constraints. The embedding step in the framework of [Panozzo et al. 2013] is based on Metric MDS [Cox and Cox 2000] and least-squares meshes [Sorkine and Cohen-Or 2004], and aims to unfold the input mesh without distorting the original triangles significantly. Since this is exactly what we want to achieve in our canonical poses, we find it meaningful to compare our result with their embedding. Our result (Fig. 7-fourth row) respects the original shape details much more than [Panozzo et al. 2013] does (Fig. 7-third row), which implies that their algorithm can be improved by employing our unfolding technique. We also show another unfolding by the well-known Landmark MDS method [de Silva and Tenenbaum 2002], which led to the worst result in terms of shape preserving (Fig. 7-second row).

4.2.2 Quantitative Evaluation. We measure the percentage of stretching (S) by comparing the maximum geodesic distances before (g_0) and after (g_1) our canonical pose computation:

$$S = \left[100 \frac{g_1 - g_0}{g_0} \right]. \quad (7)$$

Due to the nature of the unfolding task, we observe stretching to a certain extent that is controlled by parameter α in Eq. 4 (see Table I). We fix this value to 5K in most of the experiments while noting that the lower values allow further stretches. Models of the glasses class, for instance, overstretch with the usual value of $\alpha = 5K$. We consequently obtain a more plausible unfolding with more powerful edge springs imposed by $\alpha = 20K$, as illustrated in Fig. 8. Note that, the executable of our algorithm takes this tuning parameter α from the command prompt, which enables users to progressively update the value if necessary.

We also measure the similarity between the pairwise Euclidean distances at the computed canonical pose (E) and the correspond-

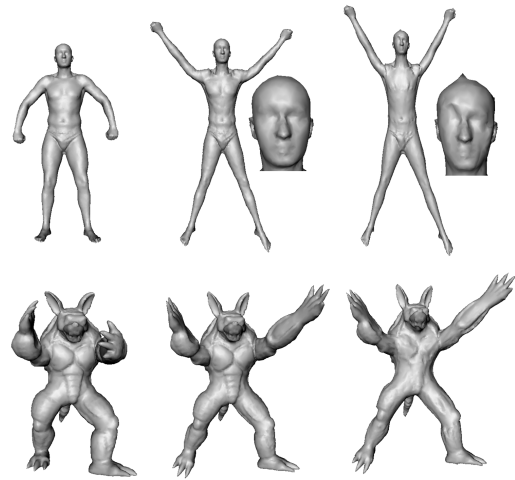


Fig. 6. SCAPE (top) and armadillo (meshes) at left are brought to their canonical poses with (middle) and without (right) the finite element constraints in Eqs. 5 and 6. Absence of constraints causes detail loss (chests) and distortion (heads) as well as additional stretching.

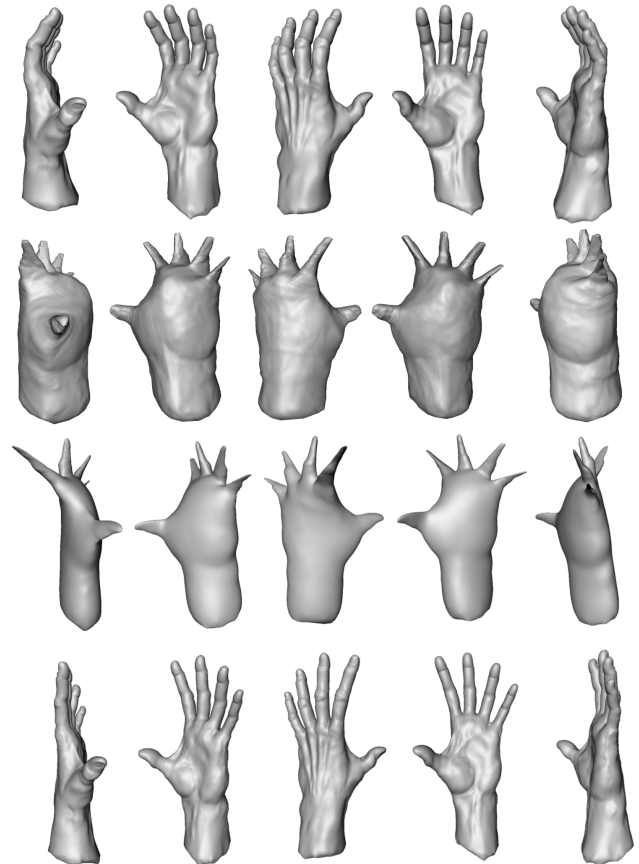


Fig. 7. Original hand model (top) is unfolded with, from top to bottom, [de Silva and Tenenbaum 2002], [Panozzo et al. 2013], and our method.

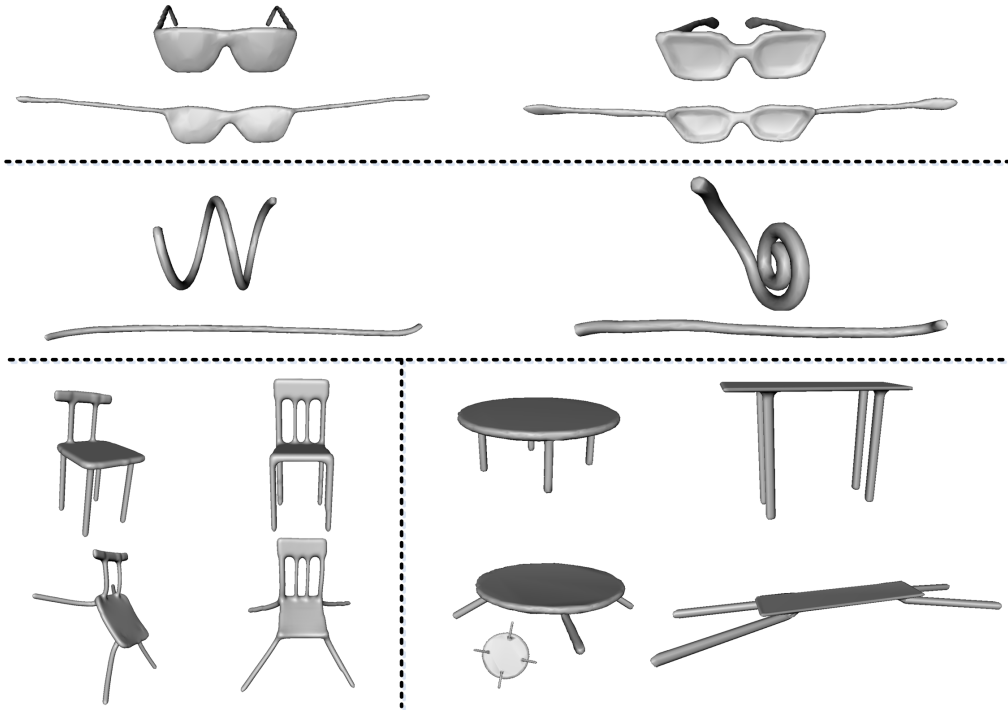


Fig. 4. Two examples of input mesh (top) and its resulting canonical pose (bottom) for each non-animal class of Watertight dataset.

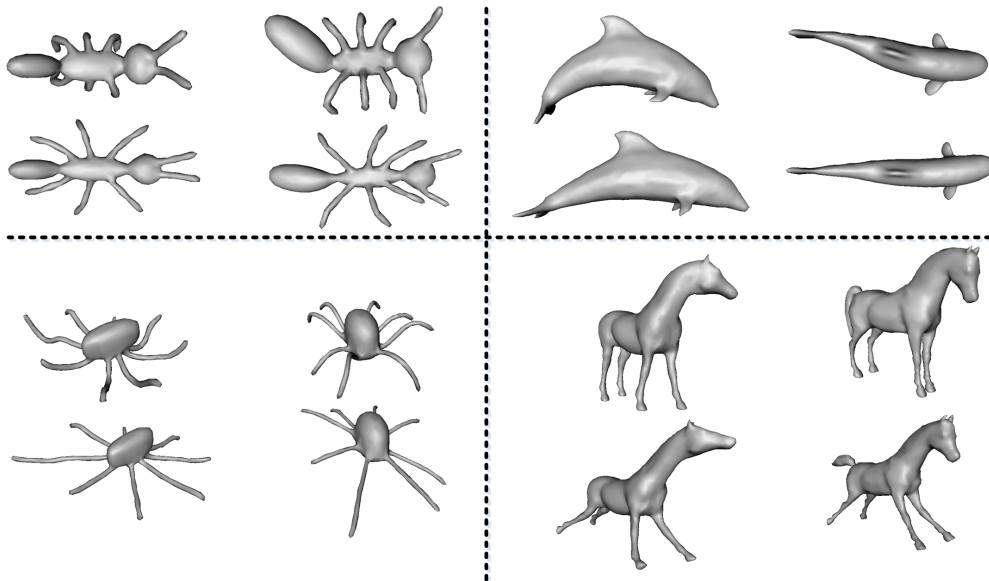


Fig. 5. Two examples of input mesh (top) and its computed canonical pose (bottom) for each animal class of Watertight dataset.

ing geodesic distances on the manifold (\mathbf{G}) via:

$$\mathcal{A} = \left\| \frac{\mathbf{E}}{\|\mathbf{E}\|_F} - \frac{\mathbf{G}}{\|\mathbf{G}\|_F} \right\|_F, \quad (8)$$

where values close to 0 imply a good geodesic approximation as the difference is taken between unit matrices. Visual inspec-

tion of this approximation is made in Fig. 9 by running [de Silva and Tenenbaum 2002] based on the standard affinity matrix \mathbf{G} , i.e., pairwise geodesic distances, and our affinity matrix \mathbf{E} , i.e., pairwise Euclidean approximations of geodesic distances. Namely, $\mathbf{G}_{i,j} = g(i, j)$ and $\mathbf{E}_{i,j} = \|\mathbf{v}_i - \mathbf{v}_j\|$. Recall that [de Silva and Tenenbaum 2002] uses M leading eigenvectors of the affinity ma-

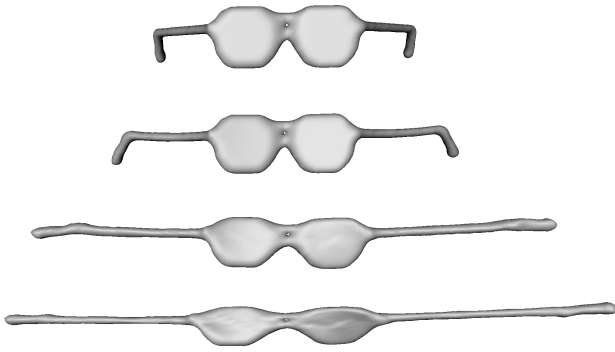


Fig. 8. Original glasses model (top) understretches with $\alpha = 100K$ (second row), overstretches with $\alpha = 5K$ (fourth row), and unfolds well with $\alpha = 20K$ (third row).

Table I. Stretching percentages S and geodesic approximation error \mathcal{A} after canonical pose optimization. A: glasses, B: ant, C: chair, D: octopus, E: table, F: fish, G: rope, H: armadillo, I: fourleg, J: SCAPE, K: hand.

	Aa	B	C	D	E	F	G	H	I	J	K
S	11	13	4	7	7	12	14	13	11	14	6
\mathcal{A}	.55	.46	.71	.74	.66	.50	.40	.51	.57	.44	.62

trix to obtain an M -dimensional spectral embedding of landmark points, and then computes embedding coordinates for the remaining data points based on their distances from the landmarks. Visual similarity between the middle and left columns of Fig. 9 is therefore another sign that Euclidean distances in our resulting canonical pose efficiently approximate geodesic distances locally on the manifold. Finally, the correlation between S and \mathcal{A} suggests that the more we allow stretching, the better the geodesic distances are approximated.

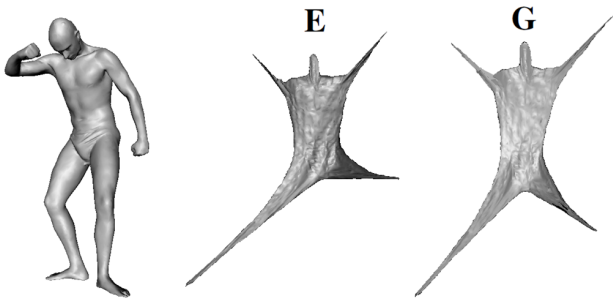


Fig. 9. Landmark MDS embeddings [de Silva and Tenenbaum 2002] of the input pose (left) based on affinity matrices \mathbf{E} (our geodesic approximation, middle) and \mathbf{G} (original geodesics, right).

Our resulting canonical poses are invariant to non-rigid transformations, that is, all articulated shapes are expected to converge to the poses that may differ by purely rigid transformations. This fact encourages us to implement a simple shape correspondence method that takes two shapes S and T , unfolds them with our method, resolves the rigid transformation ambiguity by PCA alignment [Kazhdan 2007] followed by standard ICP [Besl and McKay

1992], and matches the closest points between the aligned shapes. We demonstrate the moderate quality of a resulting correspondence in Fig. 10-top row, and note that one may infer more correspondences from the unfolded pairs of Figures 4-5. We also define the following ground-truth distortion \mathcal{D} to measure the deviation of a correspondence $\phi : S \rightarrow T$ from the ground-truth:

$$\mathcal{D}(\phi) = \frac{1}{|\phi|} \sum_{(i,j) \in \phi} g(\vartheta(i), j), \quad (9)$$

where $\vartheta(i)$ stands for the ground-truth correspondence of source vertex $i \in S$ on target T as known a priori for the SCAPE dataset. The maximum geodesic distance on the target model is normalized to 1 in order to simplify the interpretation of this measure. We observe average $\mathcal{D} = 0.178$ for 20 random pairs from the SCAPE, which is worse than the state-of-the-art non-rigid correspondence algorithms [Ovsjanikov et al. 2010; Sahillioğlu and Yemez 2013], yet accurate enough to initiate a pose-independent shape retrieval technique. After representing the query and database shapes with their canonical poses, we perform pairwise matchings between query and database as described above. We then measure shape similarities using the correspondence cost descriptor of [Jain and Zhang 2007], which is,

$$\mathcal{D}'(\phi) = \frac{1}{|\phi|} \sum_{(i,j) \in \phi} \|\mathbf{v}_i - \mathbf{v}_j\|, \quad (10)$$

where query vertex i maps to the database model vertex j after pairwise matching, and the maximum term in the summation is normalized to 1. These similarity scores, as shown under Fig. 10, intuitively take smaller values when matching a query to semantically equivalent articulated shapes since the canonical pose representations of both shapes in this scenario will be very similar. Ranking based on \mathcal{D}' yields the result set for pose-independent shape retrieval (Fig. 10). By comparing the middle and bottom rows of Fig. 10, we verify the main motivation of this paper. As we claimed in Sec. 1, similar objects with varying geometric details, such as a human and an armadillo, could not be well distinguished by a canonical pose that distorts details, such as least-squares MDS [Elad and Kimmel 2003] (Fig. 10-bottom row).

In addition to the correspondence cost descriptor (Eq. 10) for solving the pose-independent retrieval problem, we employ a compact shape descriptor extracted from the resulting canonical form. Specifically, we implement the visual-similarity based Clock Matching Bag-of-Features (CM-BOF) approach [Lian et al. 2010] in order to i) make the comparisons in Sec. 4.2.3 fair and ii) achieve faster retrieval performance than the original correspondence-based approach. For shape similarity comparison with CM-BOF, we begin with the same PCA-based pose normalization [Kazhdan 2007] between the canonically-posed query and the canonically-posed database model. Since each database model is already equipped with an histogram of visual word occurrences in an off-line process, the only task remaining is to extract the corresponding histogram on the query shape. To this end, SIFT features [Lowe 2004] computed on each of the several different views of the query is quantized against the visual vocabulary, which in turn represents the query as a histogram of visual word occurrences, and enables comparison with the database histogram. Once canonical forms are computed, a pair of shapes with 9K tetrahedra is compared with CM-BOF approach in only a few milliseconds, whereas the correspondence-based approach takes about a second. Both approaches achieve similar and satisfactory performances in retrieval accuracy (Tables II and III).

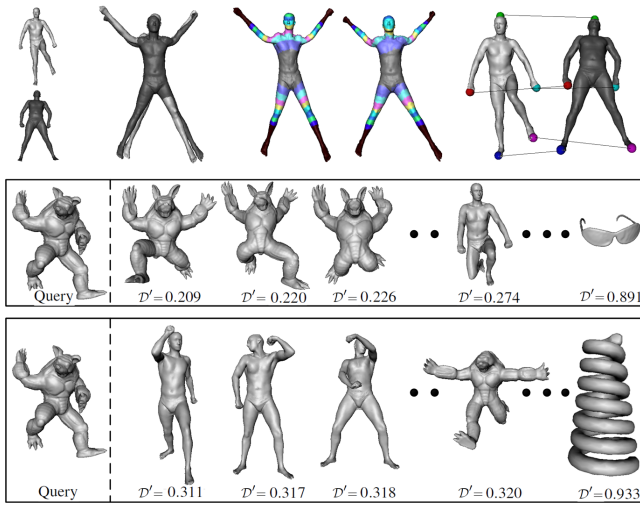


Fig. 10. Shape correspondence (top row) and retrieval (middle row) applications based on the computed canonical poses. Notice the distortion in the transfer of colors based on the computed correspondences. This inaccuracy can, however, be compensated in a retrieval application. Notice also the advantage of using our detail-preserving canonical pose (middle row) over a detail-oblivious canonical pose [Elad and Kimmel 2003] (bottom row) in discriminating an armadillo and a man.

Table II. Retrieval performances in terms of NN, 1-tier, and 2-tier metrics on our large database of 507 models. Query and database models are compared via Eq. 10.

Canonical Pose Creation	NN	1-tier	2-tier
Our method	99.1	90.2	97.3
Least-squares MDS [Elad and Kimmel 2003]	96.4	82.8	87.5
Classical MDS [Elad and Kimmel 2003]	91.4	75.8	79.9

The average execution time of our canonical pose optimization algorithm on a 2.53GHz PC for SCAPE dataset, whose models have 45K tetrahedra, is 985 seconds. The hand model with 51K tets takes 1684 seconds to get unfolded into its canonical pose. When the number of tets drops to 35K, 20K, 9K, and 3K for various Waternight models, our method demands 575, 280, 21, and 4 seconds, respectively. Note that the number of iterations, and hence the execution times, depend highly on the spatial distance between the original pose and the canonical pose to be computed.

4.2.3 Visual and Quantitative Comparisons. We first evaluate our non-rigid retrieval accuracy on our large database of 507 models using three commonly used performance metrics, namely the Nearest Neighbor (NN), which is the percentage of the first-closest matches that belong to the query class, and the First Tier (1-tier), which is the ratio of the relevant matches to the size of the query class C when the number of retrieved models, i.e., top K matches, is $|C|$. We relax $K = 2|C|$ to obtain the Second Tier (2-tier) metric. The retrieval method leading to the results in Table II converts each shape to its detail-preserving (Table II-first row) or detail-oblivious (Table II-second and third rows) canonical poses and then compares query with the database rigidly via Eq. 10. Our high NN value indicates the potential of our algorithm in a classification application. Table III is created the same way as Table II except CM-BOF is used instead of Eq. 10 for shape comparison.

Table III. Retrieval performances in terms of NN, 1-tier, and 2-tier metrics on our large database of 507 models. Query and database models are compared via CM-BOF.

Canonical Pose Creation	NN	1-tier	2-tier
Our method	99.2	89.9	97.5
Least-squares MDS [Elad and Kimmel 2003]	96.1	82.4	87.6
Classical MDS [Elad and Kimmel 2003]	91.2	75.1	79.7

Table IV. Retrieval performances in terms of NN, 1-tier, and 2-tier metrics on the McGill database. Query and database models are compared via CM-BOF.

Canonical Pose Creation	NN	1-tier	2-tier
Our method	99.7	92.1	98.6
[Lian et al. 2013]’s method	99.6	86.6	95.3
Least-squares MDS [Elad and Kimmel 2003]	98.1	80.9	86.9
Classical MDS [Elad and Kimmel 2003]	95.2	75.1	80.9

We next pass to the McGill database in order to make fair comparisons with the only other detail-preserving canonical pose method in the literature [Lian et al. 2013]. Since we are unable to reproduce the complicated algorithm described in [Lian et al. 2013], we directly import their visuals and quantifications obtained on the McGill database. In their comprehensive comparisons with the existing methods, they outperform the state-of-the-art of the non-rigid retrieval approaches that utilize MDS canonical poses, which implies that performing better than [Lian et al. 2013] would put us in front of those methods as well. We employ the same performance metrics, which are NN, 1-tier, 2-tier, and Precision-Recall, and use the same shape comparison protocol, namely the CM-BOF approach (Table IV). For the Precision-Recall plots in Fig. 11, the vertical axis is the Precision, which is the ratio of the relevant matches to the number of retrieved models, whereas the horizontal axis is the Recall, which is the ratio of relevant matches to the size of the query class. Ideally, this curve should be a horizontal line at unit precision. In addition to the plot associated with our method, we provide plots for the other canonical-based retrieval methods, namely [Lian et al. 2013] and least-squares MDS. These retrieval methods all apply the same protocol described in the first paragraph of this section. We also provide the plot of a descriptor-based method, which directly compares the low-dimensional heat-kernel signatures [Sun et al. 2009] of the query and database models, as done in [Bronstein et al. 2011]. The lower performance of the descriptor-based approach supports our claim in the Sec. 1 that canonical-based methods are more promising than descriptor-based counterparts as the canonical form can easily be integrated into a simpler and well-studied rigid shape retrieval process.

The main reason of our success over the closest work [Lian et al. 2013] is our resulting canonical pose that is more smooth and accurate in terms of unfolding the object, as shown in Fig. 12. We also note that the reported execution time of [Lian et al. 2013] for canonical pose creation of a model with 10K triangles is 243 seconds, whereas we perform the same task in about 10 seconds on a similar computer, which effectively makes our method more scalable. Finally, we are more robust to topological noise, e.g., a “short circuit” in the feet, than [Lian et al. 2013] as we avoid the use of geodesic distances. We empirically show this robustness by adding 10 virtual edges between random point pairs of each McGill model and re-running our retrieval method, which achieved almost the same performance in Table IV. Besides we display the effect of topological noise on a SCAPE model in Fig. 13, where we also demonstrate the unfolding result on a low-resolution and non-uniformly

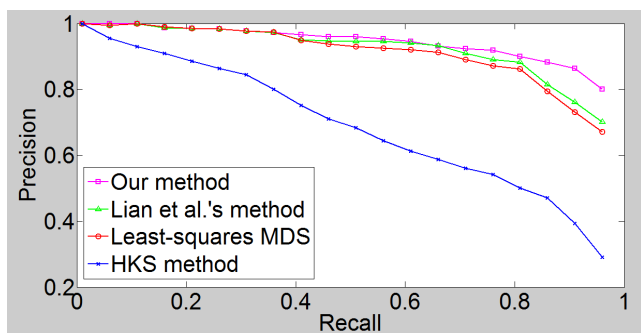


Fig. 11. Precision-recall plot of the retrieval methods.

sampled mesh (1.5K irregular tetrahedra) in an attempt to show that different versions of a 3D mesh with different resolutions can have similar canonical poses using the proposed method with the same parameters and settings, e.g., $\alpha = 5K$ in Eq. 4. As verified in Fig. 13-bottom, neither the amount (resolution) nor the quality (sampling) of the tetrahedra in the input mesh degrades the performance of our method.

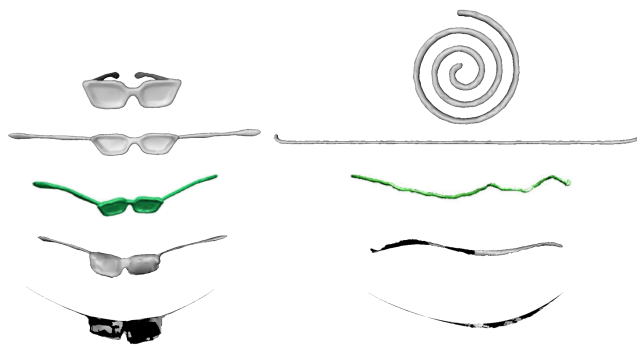


Fig. 12. Unfolding of two objects (top rows of the left and right columns) using our method (second row), [Lian et al. 2013] (third row), least-squares MDS (fourth row), and classical MDS (fifth row). Third row images are taken from [Lian et al. 2013].

4.3 Limitations

Regardless of the original pose we start with, our algorithm always converges to an unfolded canonical pose that may facilitate applications such as pose-independent shape retrieval, geodesic distance approximation, and texture mapping [Zigelman et al. 2002], to name a few. However, we have to note that our regularization scheme makes the method slightly sensitive to the original pose in that one may observe global and/or local effects of the input on the output (Fig. 14), which decreases the performance of a potential shape correspondence algorithm. We, however, show that such a loose correspondence can still be very useful in a shape retrieval framework.

5. CONCLUSION

We have introduced a shape deformation algorithm that aims to unfold a given deformable model without distorting its geometric details. This detail-preserving unfolding leads to a canonical pose that

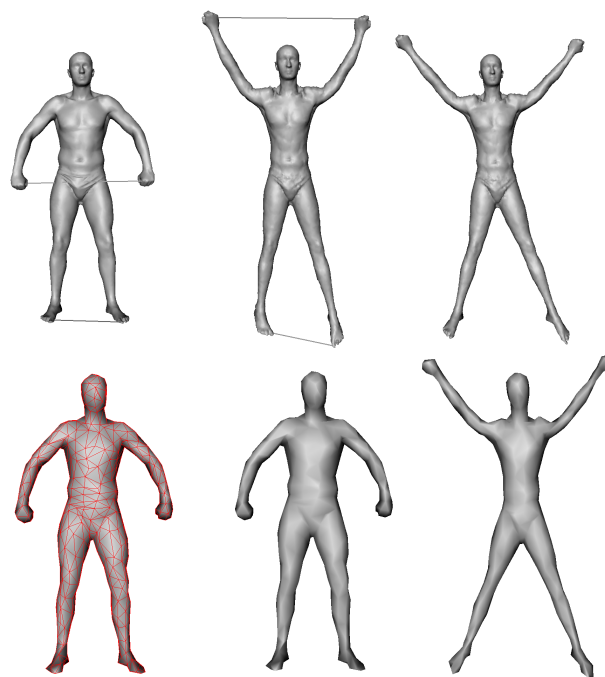


Fig. 13. (Top row) SCAPE model with topological noise on hands and feet (left) is unfolded to a model (middle) that is close to the unfolding of a noise-free input (right). (Bottom row) Low-resolution mesh with irregular tetrahedra (left and right) is unfolded to a model (right) that is close to the unfolding of a high-resolution input (top row-right).

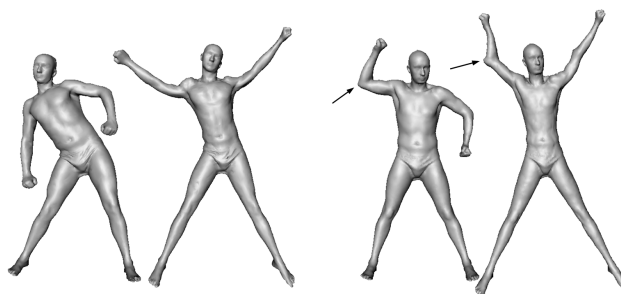


Fig. 14. Global (left pair) and local (right pair) similarities between original and canonical poses.

is invariant to non-rigid transformations and consequently suitable for non-rigid shape retrieval. We compute this canonical pose by minimizing an energy functional whose solution moves each mesh point as far away from each other as possible with respect to some regularization constraints. Our method proves useful, not only for detail-preserving mesh unfolding, but also for pose-independent shape retrieval as well as efficient approximation of geodesic distances. It is also less sensitive to topological noise and works for models of arbitrary genus. A potential application for future work may be handling different scenarios of the shape retrieval problem, such as real-time or partial retrieval. As another future work, we plan to incorporate semantic parameters into our framework so as to create more specific poses such as the Vitruvian Man pose that suggests, for instance, foot to be one-seventh of the height of a man.

Acknowledgement

We thank the anonymous reviewers for their constructive comments, and Norm Badler, James O'Brien, Tiantian Liu, Mark Pauly and Lifeng Zhu for fruitful discussions. This work was supported by TUBITAK under the project EEEAG-115E471, and the NSF awards IIS-1622360 and IIS-1350330.

REFERENCES

- ADAMS, B., OVSJANIKOV, M., WAND, M., SEIDEL, H.-P., AND GUIBAS, L. 2008. Meshless modeling of deformable shapes and their motion. *Proc. SCA*.
- ANGUELOV, D., SRINIVASAN, P., KOLLER, D., THRUN, S., RODGERS, J., AND DAVIS, J. 2005. Scape: Shape completion and animation of people. *ACM Trans. Graph.* 24, 3, 408–416.
- ASSFALG, J., BERTINI, M., AND DELBIMBO, A. 2007. Content-based retrieval of 3d objects using spin image signatures. *Trans. Multimedia* 9, 3, 589–599.
- AU, O. K.-C., COHEN-OR, D., TAI, C.-L., FU, H., AND ZHENG, Y. 2010. Electors voting for fast automatic shape correspondence. *Computer Graphics Forum (Proc. Eurographics)* 29, 2, 645–654.
- BARRA, V. AND BIASOTTI, S. 2013. 3d shape retrieval using kernels on extended reeb graphs. *Pattern Recognition* 46, 11, 2985–2999.
- BELONGIE, S., MALIK, J., AND PUZICHA, J. 2002. Shape matching and object recognition using shape contexts. *IEEE Trans. PAMI* 24, 509–523.
- BESL, P. J. AND MCKAY, N. D. 1992. A method for registration of 3D shapes. *IEEE Trans. PAMI* 14, 239–256.
- BONET, J. AND WOOD, R. 1997. *Nonlinear Continuum Mechanics for Finite Element Analysis*. Cambridge University Press.
- BOTSCH, M. AND SORKINE, O. 2008. On linear variational surface deformation methods. *IEEE Trans. Visualization and Comp. Graphics* 14, 1, 213–230.
- BRONSTEIN, A. M., BRONSTEIN, M. M., AND KIMMEL, R. 2006. Generalized multidimensional scaling: A framework for isometry invariant partial surface matching. *Proc. of the National Academy of Science* 103, 5, 1168–1172.
- BRONSTEIN, A. M., BRONSTEIN, M. M., AND KIMMEL, R. 2008. *Numerical Geometry of Non-Rigid Shapes*. Springer.
- BRONSTEIN, M., BRONSTEIN, M., GUIBAS, L., AND OVSJANIKOV, M. 2011. Shape google: geometric words and expressions for invariant shape retrieval. *ACM Trans. Graph.*
- BRONSTEIN, M. M. AND KOKKINOS, I. 2010. Scale-invariant heat kernel signatures for non-rigid shape recognition. *Proc. Computer Vision and Pattern Recognition (CVPR)*.
- BYRD, R., NOCEDAL, J., AND WALTZ, R. 2006. An integrated package for nonlinear optimization. In *Large-Scale Nonlinear Optimization* 83, 35–59.
- CHAO, I., PINKALL, U., SANAN, P., AND SCHRODER, P. 2010. Meshless deformations based on shape matching. *ACM Trans. Graph.* 29, 4.
- CHEN, D., TIAN, X., SHEN, Y., AND OUHYOUNG, M. 2003. On visual similarity based 3d model retrieval. *Computer Graphics Forum (Proc. Eurographics)* 22, 3, 223–232.
- CHEN, X., ZHENG, C., XU, W., AND ZHOU, K. 2014. An asymptotic numerical method for inverse elastic shape design. *Proc. SIGGRAPH* 33, 4.
- COX, T. AND COX, M. 2000. *Multidimensional Scaling, Second Edition*. Chapman & Hall/CRC.
- CRANE, K., WEISCHEDEL, C., AND WARDETZKY, M. 2013. Geodesics in heat: a new approach to computing distance based on heat flow. *Proc. SIGGRAPH*.
- DE SILVA, V. AND TENENBAUM, J. 2002. Global versus local methods for nonlinear dimensionality reduction. *Proc. NIPS*, 705–712.
- ELAD, A. AND KIMMEL, R. 2003. On bending invariant signatures for surfaces. *IEEE Trans. PAMI* 25, 1285–1295.
- FREIFELD, O. AND BLACK, M. J. 2012. Lie bodies: A manifold representation of 3d human shape. *Proc. European Conference on Computer Vision (ECCV)*, 1–14.
- FUNKHOUSER, T., MIN, P., KAZHDAN, M., CHEN, J., HALDERMAN, A., DOBKIN, D., AND JACOBS, D. 2003. A search engine for 3d models. *ACM Trans. Graph.* 22, 1, 83–105.
- GIORGI, D., BIASOTTI, S., AND PARABOSCHI, L. 2007. SHREC: Shape retrieval contest: Watertight models track.
- GOWER, J. C. 1966. Some distance properties of latent root and vector methods used in multivariate analysis. *Biometrika*, 325–338.
- HILAGA, M., SHINAGAWA, Y., KOHMURA, T., AND KUNII, T. 2001. Topology matching for fully automatic similarity estimation of 3d shapes. *Proc. SIGGRAPH*.
- IRVING, G., SCHROEDER, C., AND FEDKIW, R. 2007. Volume conserving finite element simulations of deformable models. *Proc. SIGGRAPH*.
- IRVING, G., TERAN, J., AND FEDKIW, R. 2004. Invertible finite elements for robust simulation of large deformation. *Proc. SCA*, 131–140.
- JACOBSON, A., KAVAN, L., AND SORKINE, O. 2013. Robust inside-outside segmentation using generalized winding numbers. *Proc. SIGGRAPH* 32, 4, 33:1–33:12.
- JAIN, V. AND ZHANG, H. 2006. Robust 3d shape correspondence in the spectral domain. *IEEE Int. Conf. on Shape Modeling and Applications (SMI)*, 118–129.
- JAIN, V. AND ZHANG, H. 2007. A spectral approach to shape-based retrieval of articulated 3d models. *Computer-Aided Design* 39, 5, 398–407.
- JOHNSON, A. AND HEBERT, M. 1999. Using spin images for efficient object recognition in cluttered 3d scenes. *IEEE Trans. PAMI* 21, 5, 433–449.
- KAZHDAN, M. 2007. An approximate and efficient method for optimal rotation alignment of 3d models. *IEEE Trans. PAMI* 29, 7.
- KAZHDAN, M., FUNKHOUSER, T., AND RUSINKIEWICZ, S. 2003. Rotation invariant spherical harmonic representation of 3d shape descriptors. *Computer Graphics Forum (Proc. SGP)*, 156–164.
- LI, B., LU, Y., LI, C., GODIL, A., AND ET AL. 2014. Shrec'14 track: Large scale comprehensive 3d shape retrieval. *Eurographics Workshop on 3D Object Retrieval*, 131–140.
- LIAN, Z., GODIL, A., AND SUN, X. 2010. Visual similarity based 3d shape retrieval using bag-of-features. *IEEE Int. Conf. on Shape Modeling and Applications (SMI)*, 25–36.
- LIAN, Z., GODIL, A., AND XIAO, J. 2013. Feature-preserved 3d canonical form. *Intl. Journal of Computer Vision (IJCV)* 102, 1-3, 221–238.
- LIPMAN, Y. AND FUNKHOUSER, T. 2009. Möbius voting for surface correspondence. *ACM Trans. Graph.* 28, 3.
- LIU, L., ZHANG, L., XU, Y., GOTSMAN, C., AND GORTLER, S. 2008. A local/global approach to mesh parameterization. *Computer Graphics Forum* 27, 5.
- LOWE, D. G. 2004. Distinctive image features from scale-invariant keypoints. *Intl. Journal of Computer Vision (IJCV)* 60, 2, 91–110.
- MAHMOUDI, M. AND SAPIRO, G. 2009. Three-dimensional point cloud recognition via distributions of geometric distances. *Graphical Models* 71, 1, 22–31.
- MITRA, N., GUIBAS, L., AND PAULY, M. 2007. Symmetrization. *Proc. SIGGRAPH* 26, 63, 1–8.
- MULLER, M., HEIDELBERGER, B., TESCHNER, M., AND GROSS, M. 2005. Meshless deformations based on shape matching. *ACM Trans. Graph.* 24, 3.

- MULLER, M., KEISER, R., NEALEN, A., PAULY, M., GROSS, M., AND ALEXA, M. 2004. Point based animation of elastic, plastic and melting objects. *Proc. SCA*, 141–151.
- NEALEN, A., MULLER, M., KEISER, R., BOXERMAN, E., AND CARLSON, M. 2006. Physically based deformable models in computer graphics. *Computer Graphics Forum* 25, 4, 809–836.
- NOVOTNI, M. AND KLEIN, R. 2003. 3d zernike descriptors for content based shape retrieval. *Proc. ACM Symposium on Solid Modeling and Applications*, 216–225.
- OSADA, R., FUNKHOUSER, T., CHAZELLE, B., AND DOBKIN, D. 2002. Shape distributions. *ACM Trans. Graph.* 21, 4, 807–832.
- OVSIJANIKOV, M., MÉRIGOT, Q., MÉMOLI, F., AND GUIBAS, L. 2010. One point isometric matching with the heat kernel. *Computer Graphics Forum* 29, 5, 1555–1564.
- PANOZZO, D., BARAN, I., DIAMANTI, O., AND SORKINE-HORNUNG, O. 2013. Weighted averages on surfaces. *Proc. SIGGRAPH*.
- PAQUET, E., RIOUX, M., MURCHING, A., NAVEEN, T., AND TABATABAI, A. 2000. Description of shape information for 2-d and 3-d objects. *Signal Proc. Image Comm.* 16, 1-2, 103–122.
- RAVIV, D., BRONSTEIN, M., BRONSTEIN, A., AND KIMMEL, R. 2010. Volumetric heat kernel signatures. *ACM Multimedia Workshop on 3D Object Retrieval*.
- REUTER, M., WOLTER, F., AND PEINECKE, N. 2006. Laplacebeltrami spectra as 'shape-dna' of surfaces and solids. *Computer-Aided Design* 38, 4, 342–366.
- RUSTAMOV, R. 2007. Laplace-beltrami eigenfunctions for deformation invariant shape representation. *Computer Graphics Forum (Proc. SGP)*, 225–233.
- SAHILLIOĞLU, Y. 2015. A shape deformation algorithm for constrained multidimensional scaling. *Computers & Graphics (To Appear)*.
- SAHILLIOĞLU, Y. AND YEMEZ, Y. 2012. Minimum-distortion isometric shape correspondence using EM algorithm. *IEEE Trans. PAMI* 34, 11, 2203–2215.
- SAHILLIOĞLU, Y. AND YEMEZ, Y. 2013. Coarse-to-fine isometric shape correspondence by tracking symmetric flips. *Computer Graphics Forum* 32, 1, 177–189.
- SCHULLER, C., KAVAN, L., PANOZZO, D., AND SORKINE-HORNUNG, O. 2013. Locally injective mappings. *Computer Graphics Forum (Proc. SGP)* 32, 5.
- SIDDIQI, K., ZHANG, J., MACRINI, D., SHOKOUFANDEH, A., BOUIX, S., AND DICKINSON, S. 2008. Retrieving articulated 3-d models using medial surfaces. *Machine Vision and Applications* 19, 4, 261–275.
- SKOURAS, M., THOMASZEWSKI, B., BICKEL, B., AND GROSS, M. 2012. Computational design of rubber balloons. *Computer Graphics Forum* 31, 2, 835–844.
- SORKINE, O. AND ALEXA, M. 2007. As-rigid-as-possible surface modeling. *Computer Graphics Forum (Proc. SGP)*, 109–116.
- SORKINE, O. AND COHEN-OR, D. 2004. Least-squares meshes. *Proc. Shape Modeling International*, 191–199.
- SORKINE, O., COHEN-OR, D., LIPMAN, Y., ALEXA, M., ROSSL, C., AND SEIDEL, H.-P. 2004. Laplacian surface editing. *Proc. Eurographics/ACM SIGGRAPH Symposium on Geometry Processing*, 179–188.
- STOMAKHIN, A., HOWES, R., SCHROEDER, C., AND TERAN, J. 2012. Energetically consistent invertible elasticity. *Proc. SCA*.
- SUN, J., OVSIJANIKOV, M., AND GUIBAS, L. 2009. A concise and provably informative multi-scale signature based on heat diffusion. *Computer Graphics Forum* 28, 5.
- TANGELDER, J. AND VELTKAMP, R. 2008. A survey of content based 3d shape retrieval methods. *Multimedia tools and applications* 39, 3, 441–471.
- TWIGG, C. AND KAČIĆ-ALESIĆ, Z. 2011. Optimization for sag-free simulations. *Proc. SCA*.
- WANG, H., SIDOROV, K., SANDILANDS, P., AND KOMURA, T. 2013. Harmonic parameterization by electrostatics. *ACM Trans. Graph.* 32, 5.
- ZAHARESCU, A., BOYER, E., VARANASI, K., AND HORAUD, R. 2009. Surface feature detection and description with applications to mesh matching. *Proc. Computer Vision and Pattern Recognition (CVPR)*, 373–380.
- ZHANG, C. AND CHEN, T. 2001. Efficient feature extraction for 2d/3d objects in mesh representation. *IEEE International Conference on Image Processing* 3.
- ZIGELMAN, G., KIMMEL, R., AND KIRYATI, N. 2002. Texture mapping using surface flattening via multidimensional scaling. *IEEE Trans. Vis. & Comp. Graphics* 8, 198–207.